PITTING CORROSION OF TiN-COATED STAINLESS STEEL IN 3 % NaCl SOLUTION

JAMIČASTA KOROZIJA NERJAVNEGA JEKLA S PREVLEKO TiN V 3-ODSTOTNI RAZTOPINI NaCl

Israfil Kucuk, Cevat Sarioglu

Marmara University, Dept. of Metallurgical and Materials Engineering, Göztepe kampusu, 34722 Kadiköy-Istanbul, Turkey
cevat.sarioglu@marmara.edu.tr

TiN coatings deposited by arc PVD were characterized by XRD and SEM. In-situ measurements of the corrosion of the substrate and the TiN-coated substrate were made using the corrosion potential (Cor.Pot.), the polarization resistance (PR) method and electrochemical impedance spectroscopy (EIS) in a 3 % NaCl solution as a function of the immersion time. The semiconductor scale formed on the TiN was identified using a Mott-Shottky analysis as an n-type semiconductor with a flat band potential of –0.83 V vs. SCE. The TiN coating (0.5 μm thick) consisted of cubic TiN exhibiting columnar grains, pin holes, voids and porosities. The pitting corrosion of the TiN, observed visually between 1 h and 2 h, was captured by EIS and PR. The electrical circuit (EC) model used for the EIS data supported the degradation of the coating through pitting corrosion, in agreement with the visual observations. The corrosion resistance (polarization resistance) determined by the polarization resistance method (R_p) and the EIS (R_{total}) decreased suddenly during the pitting corrosion. The corrosion resistance of the TiN-coated substrate was greater than the corrosion resistance of the substrate during the approximately 24 h of exposure.

Keywords: stainless steel, TiN, coating, EIS, polarization resistance, pitting corrosion

Prevleka TiN, nanesena z obločnim PVD-postopkom, je bila pregledana z XRD in SEM. In-situ meritve korozije podlage in podlage s prevleko iz TiN so bile izvršene z metodo korozijskega potenciala (Cor.Pot.), polarizacijske upornosti (PR) in z elektrokemijsko impedančno spektroskopijo (EIS) v 3-odstotni raztopini NaCl v odvisnosti od časa namakanja. Mott-Shottkyjeva analiza je odkrila nastanek n-tipa polprevodne škaje na TiN s potencialom ravnih nivojev –0.83 V proti SCE. Prevleko TiN (debeline 0,5 μm) sestavljajo kubični TiN s stebrastimi zrni, luknjami, prazninami in poroznostjo. Vidno odkrita jamičasta korozija TiN, opažena med 1 h in 2 h, je bila posneta z EIS in PR. Model električnega tokokroga (EC), ki je bil uporabljen za EIS-podatke, podpira degradacijo prevleke z jamičasto korozijo, skladno z vizualnimi opažanji. Korozijska upornost (polarizacijska upornost), določena z metodo polarizacijske upornosti (R_p) in EIS (R_{total}) se je nenadno zmanjšala med jamičasto korozijo. Korozijska upornost podlage z nanosom TiN je bila večja kot korozijska obstojnost podlage med izpostavitvijo okrog 24 h.

Ključne besede: nerjavno jeklo, TiN, prevleka, EIS, polarizacijska upornost, jamičasta korozija

1 INTRODUCTION

Hard ceramic coatings such as TiN have been used mainly for tribological applications, such as cutting tools. The tribological properties of single-layer and multi-layer TiN coatings were extensively studied in the literature and published in a handbook.[1–8] On the other hand, the corrosion of TiN in tribological applications was often overlooked, mainly due to the shorter life time of the cutting tools. TiN, with its golden colors, has been used for decorative applications, such as watches, architectural materials and ornaments. The corrosion resistance of the TiN coating is required for these decorative applications in addition to the wear resistance.

The pitting corrosion of the TiN coating deposited on the metallic substrates AISI 304, 430 and steel was observed for different coating thicknesses, exposure times and coating techniques.[9–16] Even though the widely accepted pitting corrosion mechanism of the TiN-coated substrate in the literature was local galvanic corrosion through the galvanic coupling of the TiN coating and the substrate, there remain questions about the mechanism of pitting formation and the growth of the pitting corrosion. One of the key parameters for galvanic corrosion is defects in the coatings, such as pin holes and micro and macro porosities in the coatings. The defects in the coatings provide the electrolyte with a path to the coating/substrate interface.[9–16]

Martensitic stainless steels (EN 1.4034 was used in this work) that are generally used for the blades in kitchen appliances were coated for both decorative and wear-resistance requirements. The pitting corrosion of the TiN coating deposited by arc PVD on a stainless-steel substrate was studied in detail with the corrosion potential (Cor.Pot), the polarization resistance (PR) and electrochemical impedance spectroscopy (EIS) techniques. The mechanism of the pitting corrosion was evaluated with respect to the microstructure of the TiN coating.

2 EXPERIMENTAL PROCEDURES

The substrate material obtained from ThyssenKrupp was EN 1.4034 (X46Cr13) stainless steel. The TiN

coating of the substrates was performed in an industrially sized arc PVD coating chamber (AFS ltd. Cop., Turkey). The details about the specimen preparation prior to the coating and the coating procedure are given in detail in[17]. The substrate was coated with a Ti interlayer for 1 min to improve the adhesion of the coating and later with a TiN layer for 20 min at $1.1 \cdot 10^{-3}$ mbar of nitrogen pressure and a total pressure of 10^{-2} mbar with a bias voltage of –200 V. The final deposition temperature was 250 °C.

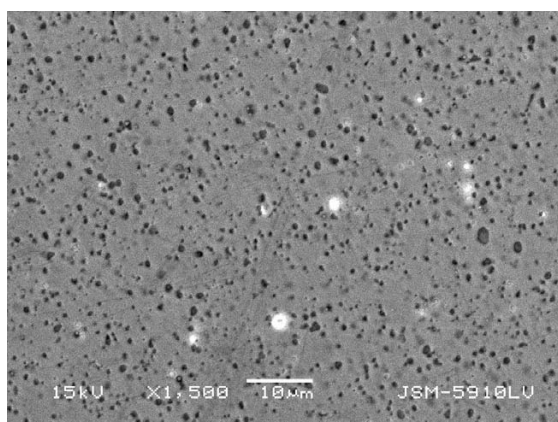The electrochemical corrosion units used to perform the EIS, the polarization resistance and the Mott-Shottky scan were a Gamry PC14/750 Poteniostat/Galvanostat/ZRA System. Details about the polarization resistance and the EIS techniques are given in[17]. All the tests were performed in 0.5 M ($w = 3$ %) NaCl aerated water solution at 25 °C using a three-electrode system (working (sample), auxiliary (graphite) and reference (standard calomel electrode (SCE)) using a Gamry paint cell unit. The Mott-Shottky analyses at a frequency of 1 Hz between +430 mV and –570 mV were performed on a TiN-coated substrate after the corrosion potential was stable.

Microstructural analyses were performed before and after the corrosion using a scanning electron microscope (SEM, Jeol, JSM-5910LV) and energy-dispersive spectroscopy (EDS). The cross-section of the coatings was observed after it was fractured in liquid nitrogen. X-ray diffraction (Rigaku, D-MAX 2200, Cu K_α radiation) was used to identify the structure of the coatings deposited on the substrate.
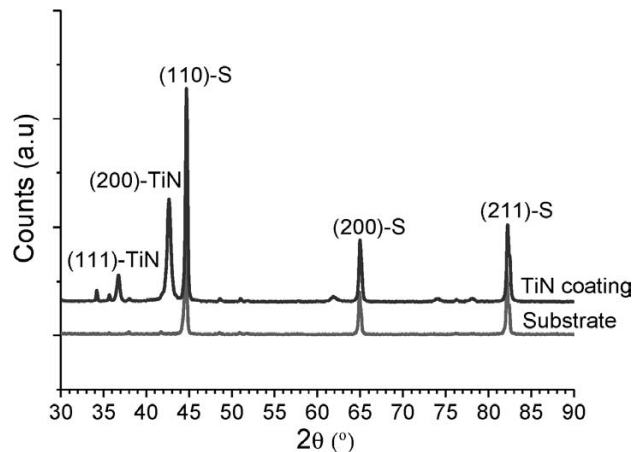
3 RESULTS

3.1 Microstructural characterization of the substrate and the TiN-coated substrate

An SEM micrograph of the microstructure of the substrate material is presented in **Figure 1**. The carbide phases (Cr and C-rich phase identified by EDS), etched

Figure 2: 2θ scan obtained from the EP 4034 steel substrate and TiN-coated substrates using the Bragg-Brentano symmetric X-ray diffraction
Slika 2: 2θ-posnetek Bragg-Brentano simetrične rentgenske difrakcije EP 4034 podlage in prevleke TiN na podlagi

Figure 3: SEM (SEI) micrographs taken from TiN-coating surface at: a) low magnification and b) high magnification. TiN coating deposited over carbide phases (dark areas) were distinguished with depression over the surface at a) and b). Embedded droplets deposited throughout the surface were marked at b). Bright particles on coating surface were un-embedded droplets (spherical particles). Pin holes were marked on surface b).
Slika 3: SEM (SEI)-posnetka površine prevleke TiN pri: a) majhni povečavi in b) veliki povečavi. Prevleka TiN je nanesena preko karbidnih faz (temna področja), ki se razpoznajo po vdolbini na površini a) in b). Vgnezdene kapljice, nanesene na površino, so označene na b). Svetli delci na površini nanosa so nevgnezdene kapljice (sferični delci). Luknjice so označene na površini b).
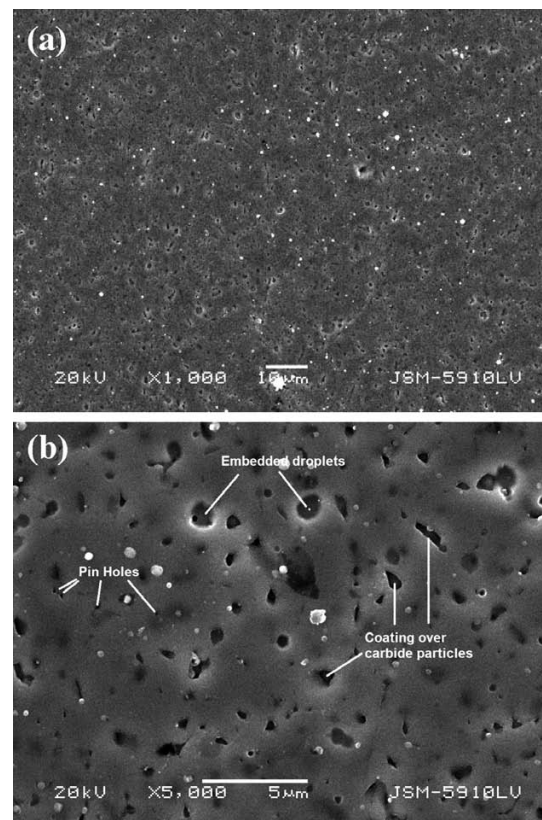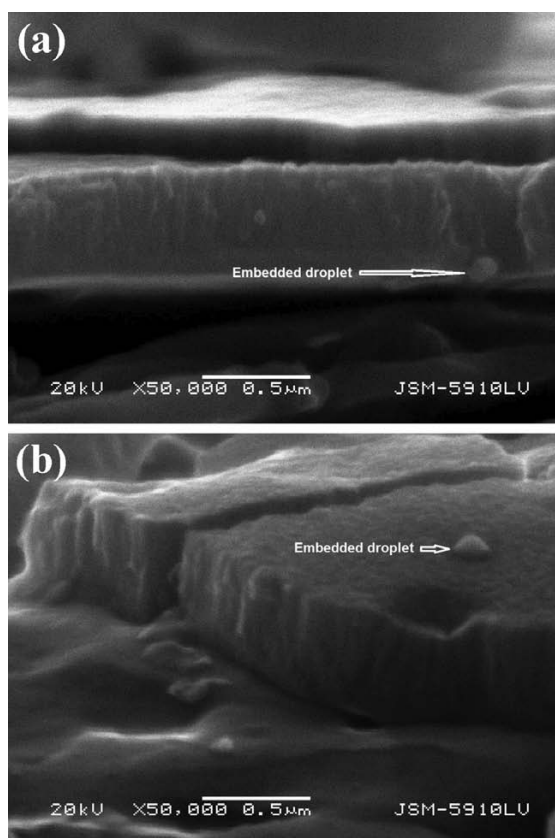

Figure 1: SEM (BEI) micrograph of EP 4034 substrate where dark-grey particles were carbides and bright phases were Fe-rich Fe-Cr particles in a grey matrix
Slika 1: SEM (BEI)-posnetek podlage iz EP 4034, kjer so temnosive pike karbidi, svetle pa faze z Fe bogati Fe-Cr-delci v sivi osnovi

Figure 4: SEM (SEI) of micrographs of fractured surface (in liquid nitrogen) of TiN coating from different areas a) and b). Columnar grains of TiN through fractured coating seen at a) and b). Embedded droplets at surface b) and at coating/substrate interface a) were marked.

Slika 4: SEM (SEI)-posnetka površine preloma (v tekočem dušiku) prevleke TiN na različnih področjih a) in b). Stebrasta zrna TiN skozi prelom prevleke se vidijo na a) in b). Na površini b) in na stiku prevleka – podlaga a) so označene vgnezdene kapljice.

slightly more than the matrix during the electropolishing treatment, were distributed homogenously throughout the matrix. The 4034 EP stainless-steel substrate possessed a ferritic structure (α-Fe), as confirmed by the XRD (**Figure 2**).

After coating with TiN at $1.1 \cdot 10^{-3}$ mbar of N_2 partial pressure, the surface morphology of the coating reflected the morphology of the EP substrate surface, where the etched carbide phases were covered by a TiN coating (**Figure 3**). The TiN coating was identified as a cubic TiN phase (**Figure 2**). Due to the arc PVD process, the droplets formed on the surface of the TiN-coated substrates. There were two different types of droplets found on the surface of the TiN coatings (**Figures 3** and **4**). One of them was the droplets embedded to the scale, i.e., the coating. These droplets were deposited and incorporated into the coatings during the coating process (**Figures 3** and **4**). The other droplets were un-embedded macro-particles (bright, spherical particles) (**Figure 3**). They were thought to be deposited on the surface through vapour-phase precipitation after the coating was

finished (when the bias was interrupted). These droplets analysed by EDS contained mainly Ti and N (Ti-rich particles). Based on a detailed surface and cross-section investigation (**Figures 3** and **4**), it was found that the TiN coating exhibited columnar grains (50 nm diameter) that were aligned perpendicular to the substrate surface (**Figure 4**) and possessed a significant amount of pin holes and porosity at the surface (**Figure 3**). The thickness of the TiN coatings, measured from the cross-section (**Figure 4**), was about 0.5 μm.

### 3.2 Corrosion of the substrate and the TiN-coated substrate

The corrosion of the substrate and the TiN-coated substrate was followed by corrosion potential, PR and EIS measurements during about 24 h of exposure. The visually observed state of the surface was noted during the corrosion evaluation. The corrosion potentials were plotted as a function of the exposure time in **Figure 5**. In general, the corrosion potential on the surface of the TiN decreased with time to a level close to the corrosion potential of the substrate material (**Figure 5**). At all times, the corrosion potential of the substrate was lower compared to the TiN coating during the approximately 24 h of exposure.

The polarization resistance measurements of the substrate and the TiN-coated substrate were performed for a period of 160 s (2.7 min) as a function of the exposure time (**Figures 6** and **7**). The polarization resistance values (R_p) were determined using the polarization resistance method and are plotted in **Figure 5**. The polarization resistance value (R_p) of the substrate determined from the plots in **Figure 6** increased gradually until it
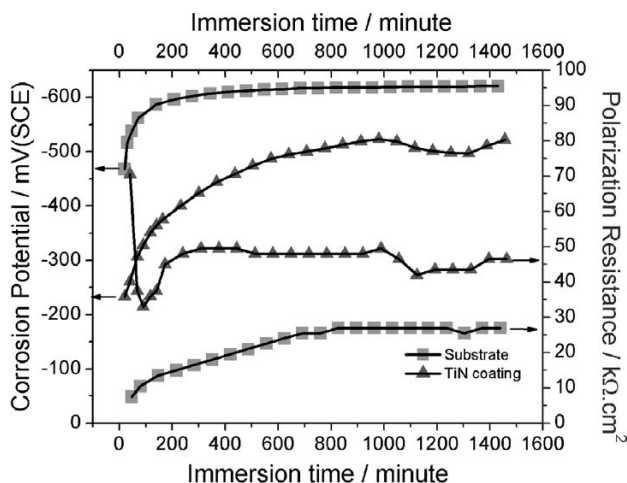
Figure 5: Corrosion potentials and polarization resistances (R_p) of the substrate and TiN-coated substrates determined from the polarization resistance scan (**Figures 6** and **7**) in 3 % NaCl solution as a function of the immersion time

Slika 5: Korozijski potencial in polarizacijska upornost (R_p) podlage in podlage s prevleko TiN so določene s posnetka polarizacijske upornosti (**sliki 6** in **7**) v 3-odstotni raztopini NaCl v odvisnosti od časa namakanja
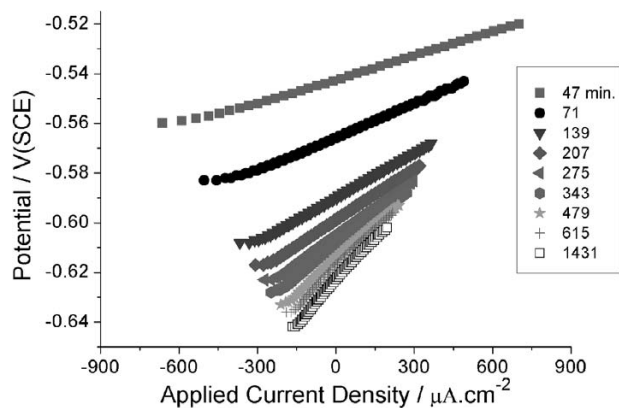
Figure 6: Polarization resistance scan of the substrate in 3 % NaCl solution as a function of immersion time
Slika 6: Zapis polarizacijske upornosti podlage v 3-odstotni raztopini NaCl v odvisnosti od časa namakanja

reached a constant value of 27 kΩ cm² after 819 min and remained at the same level until 1431 min of exposure, **Figure 5**. The polarization resistance (R_p) of the TiN coating (**Figure 5**) determined from the polarization resistance plots (**Figure 7**), exhibited a different evolution during the exposures 24 h. At the start, the polarization resistance (R_p) after 40 min decreased from 70.5 kΩ cm² to 33 kΩ cm² within 50 min and then gradually increased to 48 kΩ cm² in 300 min of exposure and stayed almost constant until 1456 min. The evolution of the polarization (R_p) is clear from the PR measurement in **Figure 7** through the expansion and contraction of the PR data. The steep drop in the polarization-resistance value during early exposure between 40 min and 90 min coincided with the visual observation of four pits formed on the surface between 80 min and 95 min of immersion time. These pits and others formed latter grew during the exposure time. During 24 hours of exposure, the corrosion resistance (polarization resistance, R_p) of the TiN-coated substrate (**Figure 5**), was greater than the corrosion resistance of the substrate.
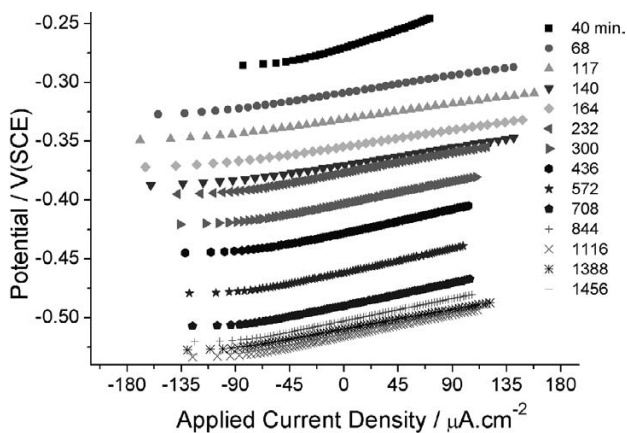

Figure 7: Polarization resistance scan of TiN coating in 3 % NaCl solution as a function of immersion time
**Slika 7:** Zapis polarizacijske upornosti prevleke TiN v 3-odstotni raztopini NaCl v odvisnosti od časa namakanja

The EIS measurements of the substrate and the TiN-coated substrate were also performed during about 24 h of exposure in a salt solution (**Figures 8** and **9**). The Bode and Nyquist plots for the substrate material were shown in **Figures 8a** and **8b**. In the Nyquist plots (**Figure 8a**), the real and imaginary impedance values gradually increased with the exposure time during the first 759 min and then stayed almost constant until 1439 min of exposure. The Bode plots (**Figure 8b**) exhibited a one-time constant with a minimum in the phase shift close to –80° and at a characteristic frequency of about 10 Hz. The magnitude of the impedance Z also increased with time, as shown for the selected exposure times in the Bode plot (**Figure 8b**).

The Bode and Nyquist plots of the TiN coatings were presented in **Figures 9a** and **9b**. The Nyquist plot (**Figure 9a**) clearly demonstrated the evolution of the real and imaginary impedance during the early exposure in the salt solution. The first measurement was performed after 40 min. In the Nyquist plot (**Figure 9a**) the impedance values dropped (shrinkage of curves) until 90 min and then started to increase up to 376 min. The evolution of the Nyquist plot took place during a visual observation of the pits (4 pits observed between 80 min and 95 min). Clearly, the pit formation and the growth of the pits at the early stage were captured by EIS measurements (particularly by the Nyquist plot, more sensitive to
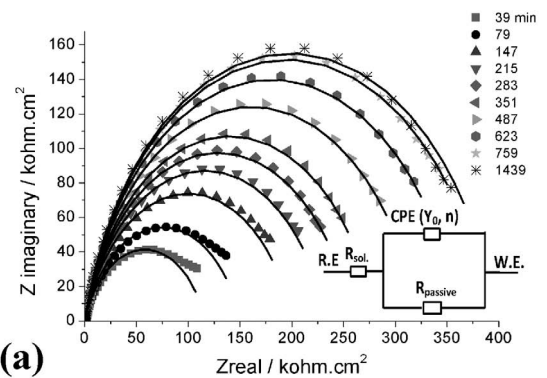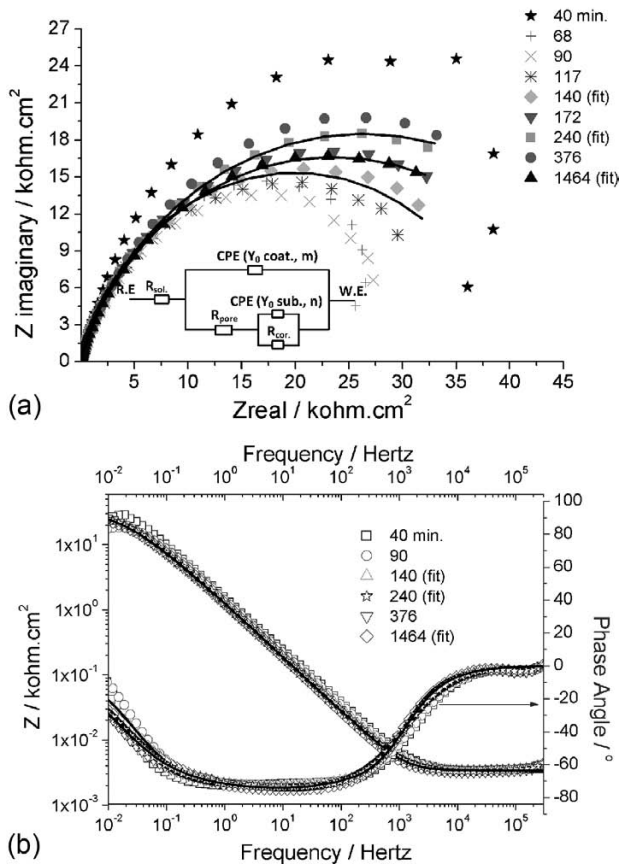

(a)
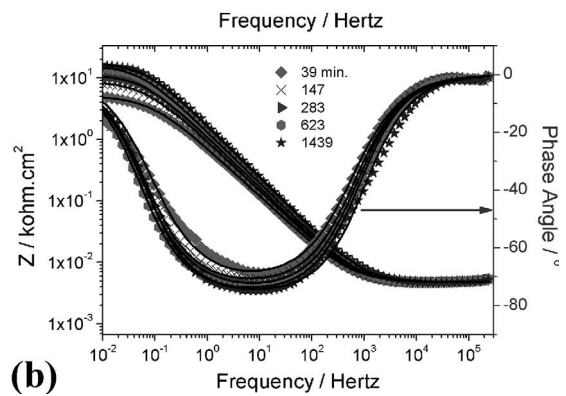
(b)

Figure 8: EIS data of the substrate for selected immersion time: a) Nyquist and b) the Bode plots
Slika 8: EIS-podatki podlage pri izbranih časih namakanja: a) Nyquistovi in b) Bodejevi diagrami

**Figure 9:** EIS data of TiN coating for selected immersion time: a) Nyquist plots and b) the Bode plots

Slika 9: EIS-podatki prevleke TiN pri izbranih časih namakanja: a) Nyquistovi in b) Bodejevi diagrami

evolution during pitting). After 376 min of exposure, the Bode and Nyquist plots did not vary significantly and the evolution of the impedance data (**Figure 9a**) resembled a polarization resistance scan (**Figure 7**).

### 3.3 Light and SEM surface examination after the corrosion

As the corrosion potentials, PR and EIS measurements were performed, the surfaces of the samples were visually observed during the exposure in the salt solution. There was no change in the colour or the pit formation on surface of the substrate. As mentioned before, at an early stage four pits were observed on the surface of the TiN-coated substrate and they grew, leaving behind circler brownish colour residues that were around these four pits. The other pits (up to 5) appeared at a later stage of the exposure and with a smaller size (lesser growth of pits). **Figure 10** shows one of the four pits formed on the surface of the TiN coating at an early stage and which grew during 1464 min of exposure. The brownish colour observed visually for the surrounding of the pits corresponded to dark-grey circles in the SEM micrograph (**Figure 10a**). A large amount of oxygen and iron elements were found in these areas by EDS analysis,

indicating the dissolution of the substrate and the formation of Fe oxide on the coating surface. **Figures 10b** and **10c** showed the same pit surface at a high magnification. In some areas, the coating was spalled off and in some areas they were detached from the substrate (**Figure 10b**). At the periphery of the pit the interior of the coating was cracked and detached from the surface (**Figure 10c**). **Figure 11** presented the substrate surface for bare areas inside the pit at a high magnification. In
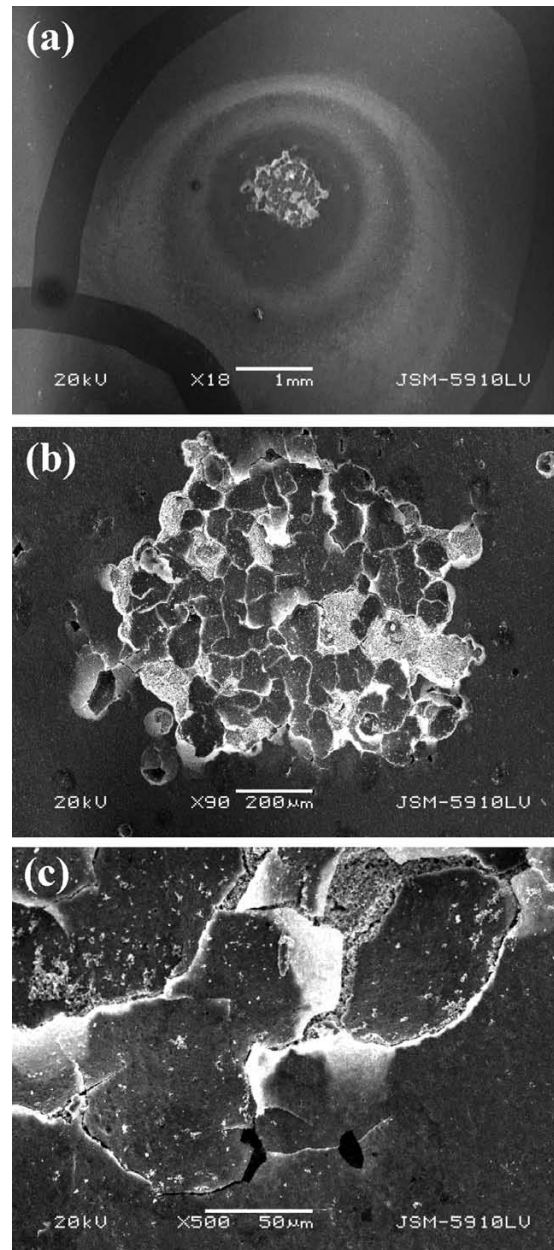
Figure 10: SEM (SEI) micrographs taken from the one of the large pits formed during early exposure: a) the micrograph of the pit marked at low magnification, b) the micrograph from the interior of the pit and c) the micrograph from the periphery of the pit interior at high magnification

Slika 10: SEM (SEI)-posnetki velike jamice, nastale v začetku namakanja: a) posnetek jamice pri majhni povečavi, b) posnetek notranjosti jamice in c) posnetek okolice jamice pri večji povečavi
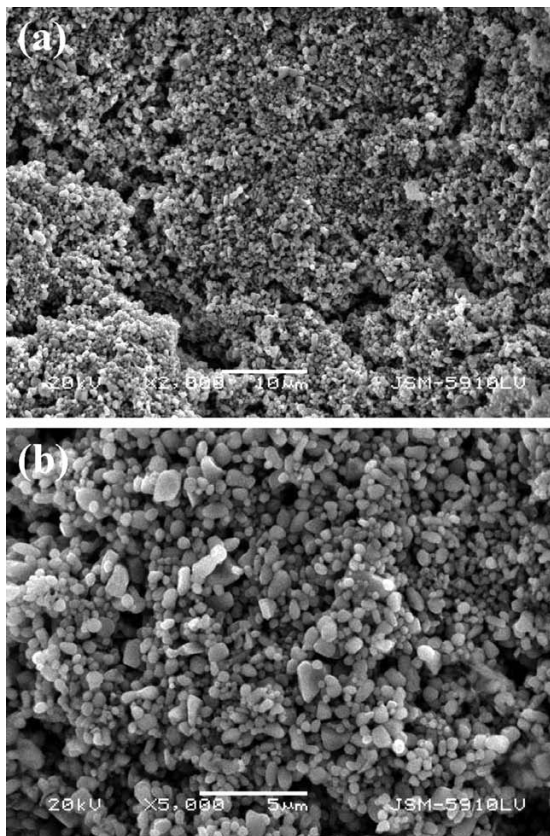
Figure 11: SEM (SEI) micrographs taken from the interior of the pit in **Figure 10** where the scale was removed: a) low magnification and b) high magnification from the same area in a). Equiaxed particles were observed on substrate surface at a) and b).
Slika 11: SEM (SEI)-posnetka okolice jamice, prikazane na **sliki 10**, kjer je bila površina odstranjena: a) majhna povečava in b) velika povečava istega področja na a). Enakoosne delce se opazi na površini podlage a) in b).

the bare areas, there were approximately diameter 1 μm round grains of pure Cr-Fe particles. These particles (**Figure 11b**), identified by EDS as Cr-rich particles
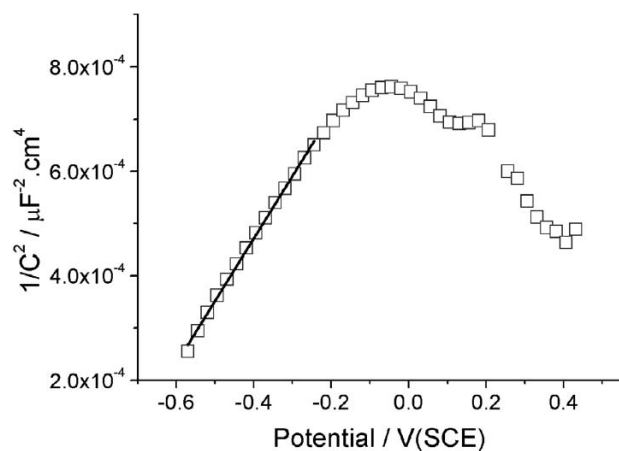
Figure 12: The Mott-Shottky measurements made for TiN coating at a frequency of 1 Hz in 3 % NaCl solution
Slika 12: Mott-Shottkyjeve meritve na prevleki TiN pri frekvenci 1 Hz v 3-odstotni raztopini NaCl

containing Fe but no oxygen and Ti, were thought to be deposited on the bare, exposed substrate surface after the experiment during the drying of the surface. The same morphological observations also were made for other pits.

3.4 The Mott-Shottky measurements

The Mott-Shottky measurements were made for the TiN coatings and plotted in **Figure 12**. Before the Mott-Shottky measurement was made, there was no pit and no colour change on the surface, the corrosion potentials were stable and the EIS data indicated strong capacitive responses at an early stage of the exposure. The Mott-Shottky plot for the TiN coatings (**Figure 12**) exhibited a linear segment between –195 mV and –570 mV vs. SCE with a positive slope. The positive slope indicated an n-type semiconductor oxide layer on the TiN surface.

4 DISCUSSION

4.1 Structure of the TiN coatings

The cubic crystal structure of the TiN was identified by XRD (**Figure 2**). In the literature, the single phase of the TiN coating was generally obtained with various N_2 pressures, since TiN was stable across a wide stoichiometric range.[11–19] The grain morphology of the TiN coating was columnar (**Figure 4**). The columnar grain boundaries in the TiN coatings, aligned perpendicularly from the topmost surface down to the substrate/coating interface (**Figure 4**), were considered to be an easy path for the penetration of the electrolyte.[19] The droplets, which were considered as a preferential site for pitting in,[9] were found on the TiN coating (**Figures 3** and **4**). The TiN coatings possessed a less uniform coverage over the etched carbide phases and droplets (**Figure 3**), resulting in a large quantity of porosity and pin holes. All these defects (columnar grain boundary, droplets, pin holes and porosities) in the coating are preferential sites for the penetration of the electrolyte during the pitting corrosion of the TiN coating.

4.2 Mott-Shottky analysis of the TiN coating

In the literature, the Mott-Shottky analysis has been used to characterize the semiconductor layer formed on the surfaces of materials and coatings.[11,16–21] Based on **Figure 12**, it was concluded that the semiconductor layer formed on the TiN-coated substrate was n-type (presumably TiO_2), in agreement with the literature.[11,21]

The Mott-Shottky equation on page 127 in[20] was used to determine the flat band potential and the density of the charge (density of donors for n-type semiconductor) in the space-charge region. After taking the dielectric constant of TiO_2 as 60, cited in[21] as[20], the flat band potentials and the density of the charges were determined from the linear portion of the plot in **Figure 12** using the eq. in[20].

The density of the donors charge in the n-type TiO_2 was $2.01 \cdot 10^{25}$ cm^{-3}. Rudenja[21] found similar values for a TiN coating deposited on 304 stainless steel as $2.4 \cdot 10^{24}$ cm^{-3} in a solution of 0.1 M H_2SO_4 and 0.05 M HCl. The calculated flat band potentials from the intercept of the plots (**Figure 12**), were –0.83 V vs. SCE for the n-type TiO_2.

4.3 Corrosion of the substrate and the TiN-coated substrate and EIS modelling

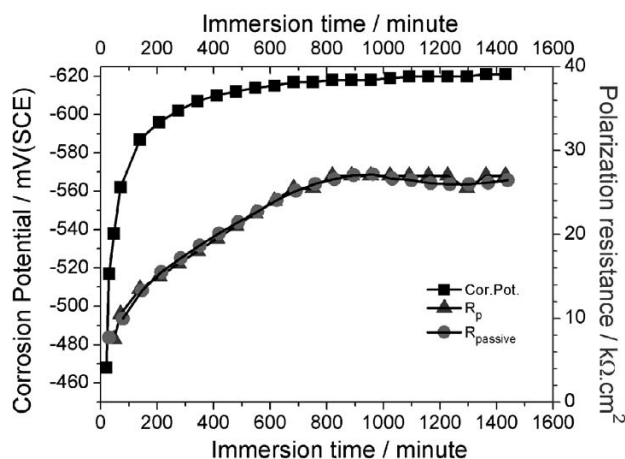The thickness of the TiN was relatively small, 0.5 μm, compared to the literature, where the thinnest coating thickness studied usually about 2 μm. For decorative applications, the coating thickness was kept as small as possible for reasons of cost (0.5 μm in this work could not be the optimum thickness). Because of this small coating thickness, a coating failure of the TiN coating (pitting) as early as about 1 h was observed. The pitting corrosion of the TiN coating at an early stage of immersion was captured by the Cor.Pot., PR and EIS measurements. In order to explain the corrosion mechanism of the TiN coating, the corrosion of the substrate and then the corrosion of the TiN coating at the early stage and later within 24 h were evaluated together with the EIS data and the EC modelling, **Figures 8** and **9** in the next section.

The EIS data of the Bode and Nyquist plots of the substrate clearly exhibited a one-time constant (particularly the phase angle vs the frequency plot in the Bode plots) during 24 h of exposure in a salt solution (**Figure 8**). It has been well known that any parallel RC circuit found in the EC represents a time constant (τ), corresponding to the characteristic frequency (ω_c).[18,19,22] Because of one time constant observation in the Bode and Nyquist plots and the absence of pitting corrosion, the EIS model (**Figure 8a**) proposed for uncoated substrates to simulate the interacting of the electrolyte with the surface consisting of a solution resistance ($R_{sol.}$) and in parallel the total resistance of the passive layer (capacitive layer), $R_{passive}$ with constant phase elements (CPE) of the passive layer. $R_{passive}$ was the resistance of the passive layer. The fit parameters, i.e., Y_0, n, $R_{sol.}$ and $R_{passive}$, were determined from the best non-linear least-square fit to the electrical circuit model with a goodness-of-fit value and they are given in **Table 1** for selected times of exposure. Also, the fitted EIS plots were given in

Figure 13: The corrosion potential (Cor.Pot.), polarization resistance (R_p and $R_{passive}$ calculated from EIS data) for the substrate in 3 % NaCl solution as a function of immersion time
Slika 13: Korozijski potencial (Cor.Pot.), polarizacijska upornost (R_p in $R_{passive}$ izračunani iz EIS-podatkov) za podlago v 3-odstotni raztopini NaCl v odvisnosti od časa namakanja

Figures 8a and **8b**. The goodness of fit (χ^2) for all the samples was in the range $1–7.6 \cdot 10^{-3}$ (**Table 1**). The error in the $R_{passive}$ and Y_0 was about 1 %. The value of $R_{passive}$ (**Figure 13**) calculated from the EIS data was the same as R_p calculated from the PR method (**Figure 5**) as expected.[22] Y_0, the admittance constant of the CPE, is a measure of the capacity (C).[23] Y_0 equals the capacity (C) when $n = 1$ for an ideal capacitor. The n value is related to the roughness and the inhomogeneity of the passive (capacitive) film and is less than 1 when the surface is rough.[17,18,23] The n value was about 0.84 (**Table 1**), and constant during the exposure, indicating that the surface roughness (surface area) did not change during the immersion.

The polarization resistance of the EP substrate (R_p and $R_{passive}$) (**Figure 13**), indicated that the resistance of the passive layer increased from 7.5 kΩ cm^2 to 27 kΩ cm^2 with the exposure time. The Y_0 was also calculated from the EC model and plotted in **Figure 14**. The Y_0 decreased with time and the variation was logarithmic with time as R_p and $R_{passive}$. The capacity values of the passive film determined from Y_0 (presumably Cr_2O_3) (**Figure 14**) decreased logarithmically, indicating that the passive film thickened with the exposure time under assumption that the dielectric property of the passive

Table 1: The EIS fit parameters of the substrate from the electrical circuit model (EC model): Y_0, n, $R_{sol.}$ and $R_{passive}$ were determined by the best non-linear least-square fit with the goodness of the fit value (χ^2)
Tabela 1: EIS-parametri podlage, pridobljeni iz modela električnega tokokroga (EC-model): Y_0, n, $R_{sol.}$ in $R_{passive}$, so bili določeni z najboljšim ujemanjem z nelinerano metodo najmanjših kvadratov in vrednostjo ujemanja (χ^2)

Immersion time (min)	$R_{sol.}$/kΩ cm^2	$R_{passive}$/kΩ cm^2	Y_0/μcm^{-2} s^n Ω	n	Goodness of fit ($\chi^2 \cdot 10^3$)
39	7.1	7.71	213.4	0.79	2.47
147	7.1	13.32	160.7	0.81	6.883
283	7.1	17.16	132.5	0.83	0.981
623	7.2	24.09	107.3	0.84	6.423
1439	7.2	26.48	82.4	0.84	7.556

Table 2: The EIS fit parameters of the TiN coating from the electrical circuit model (EC model): Y_0 coat., Y_0 sub., n, m, $R_{sol.}$, R_{pore} and $R_{cor.}$ were determined by the best non-linear least-square fit with goodness of the fit value (χ^2)
**Tabela 2:** EIS-parametri, pridobljeni za prevleko TiN iz modela električnega tokokroga (EC model): Y_0 coat., Y_0 sub., n, m, $R_{sol.}$, R_{pore}, in $R_{cor.}$, so bili določeni z najboljšim ujemanjem z metodo nelineranih najmanjših kvadratov in vrednostjo ujemanja (χ^2)

Immersion time (min)	$R_{sol.}$/Ω cm^2	R_{pore}/kΩ cm^2	$R_{cor.}$/kΩ cm^2	n	m	Y_0 (coat.)/ μcm^{-2}s^n Ω	Y_0 (sub.)/ μcm^{-2}s^n Ω	Goodness of fit ($\chi^2 \cdot 10^3$)
40	4.9	53.93	–	–	0.83	90.7	–	19.14
90	5.1	0.34	33.65	0.75	0.9	60.3	45.47	13.25
140	5.1	0.17	43.40	0.72	0.93	54.6	59.73	13.82
240	5.1	0.06	53.75	0.72	0.96	40.6	83.13	1.418
648	5.0	0.07	58.41	0.71	0.97	38.9	83.60	1.633
1124	5.2	0.05	47.78	0.73	1	30.2	84.40	1.444
1464	5.1	0.05	48.06	0.73	1	31.5	86.53	1.440

film did not change with time. The logarithmically increase in the polarization resistance (R_p and $R_{passive}$) with time verified this assumption (**Figure 13**) since (R_p and $R_{passive}$) and the current density must relate to the rate of the thickening (dx/dt).[22]

The capacitive (dielectric) layer of TiO$_2$ formed on TiN as implied by EIS data was identified with the Mott-Shottky analysis as n-type semiconductive layer and that was represented by Y_0. At an early stage of exposure, the transition from strong capacitive to less capacitive behaviour was observed in the EIS measurements (**Figure 9**). The transition for the TiN-coated substrate was a result of the pitting formation and growth. The transition was reproduced with three samples and took place between 1 h and 2 h of exposure for all the samples. Because of the pitting formation and growth at the substrate/TiN coating interface between 80 min and 95 min, after 40 min the EIS model used for the data in **Figure 9** was changed to the model employed in[18,19,24] for porous coatings and paints in order to include the pitting formation and the growth at the substrate/electrolyte interface. This model included two time constants (two

RC) (**Figure 9a**).[19,24] The goodness of the EIS data fit was in the range 1.4–19 · 10^{-3} (**Table 2**). It was higher at an early exposure time due to the dynamic change of the corrosion state (**Table 2**). As an example, three fits are shown in **Figures 9a** and **9b**. The representative data especially during pitting were tabulated in **Table 2**. During the pitting formation and growth periods R_{total} (R_{pore} + $R_{cor.}$) plotted in **Figure 15** as well as R_{pore} decreased while Y_0 sub., (admittance at substrate/electrolyte interface) increased (**Table 2**). $R_{cor.}$ was the electron charge-transfer resistance at the substrate/electrolyte interface. The decrease in the pore resistance (R_{pore}) and the total resistance, and the increase in the capacity (through Y_0 sub.) at the substrate interface implied the degradation of the coating at the interface. As observed visually, these degradations took place through the pitting formation and growth. After the pits grew to some extent, the total resistance increased slightly and stayed constant for some periods up to 12 h and then fluctuated due to the new pits being formed (five new pits were observed after 24 h) (**Figures 5** and **15**). The total polarization resistance (R_{total}) and R_p were very similar and
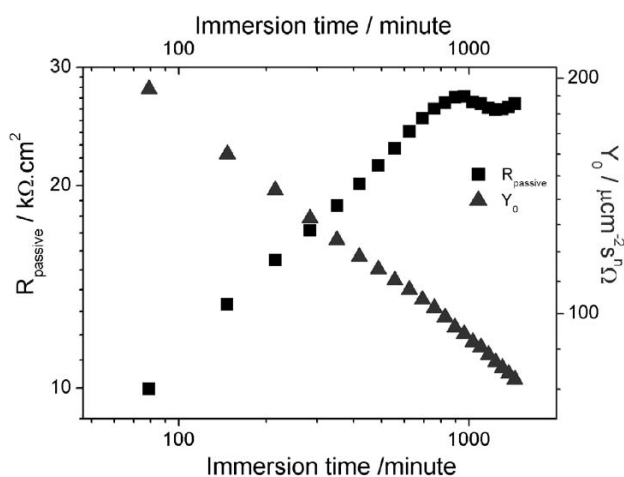
Figure 14: The admittance (Y_0) and polarization resistance ($R_{passive}$ calculated from EIS data) for the substrate in 3 % NaCl solution as a function of immersion time
Slika 14: Admitanca (Y_0) in polarizacijska upornost ($R_{passive}$ izračunana iz podatkov EIS) za podlago v 3-odstotni raztopini NaCl v odvisnosti od časa namakanja
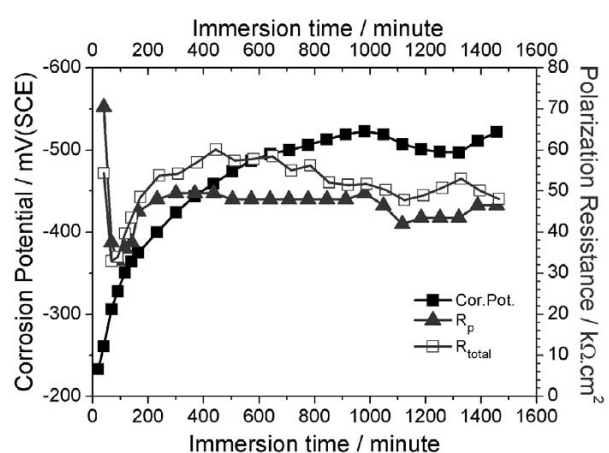
Figure 15: Corrosion potential (Cor.Pot.), polarization resistance (R_p and R_{total} calculated from EIS data) for the TiN coating in 3 % NaCl solution as a function of immersion time
Slika 15: Korozijski potencial (Cor.Pot.), polarizacijska upornost (R_p in R_{total} izračunani iz EIS podatkov) za prevleko TiN v 3-odstotni raztopini NaCl v odvisnosti od časa namakanja

followed the same trend (**Figure 15**), indicating that during the EIS measurement the corrosion state did not change significantly and caused a significant error (the PR measurement took 2.7 min, shorter than the 8 min EIS measurement).

The Y_0 coat. value, (admittance constant for TiO_2 layer) decreased continuously, while the Y_0 sub., for the substrate/solution interface stayed relatively constant for longer times (**Table 2**). After the pitting corrosion, the *n* value for the capacitive layer at substrate/electrolyte interface remained constant at low level in the range 0.72–0.76 (**Table 2**). The value of *m* for the capacitive coating on TiN was always at a high level in the range 0.9–1.0 after pitting formation, while at the beginning during the pitting formation it was 0.83, indicating that surface roughness was significant during the early exposure (during pitting) and at longer exposure times the surface became smoother. Recently, He[25] studied the in-situ AFM of exposed TiN (1 μm layer) deposited by DC reactive magnetron sputtering on 304 stainless steel in a 3.5 % NaCl solution and observed decreasing in roughness with time in first exposure 60 min. They explained this result with an in-situ observation of closing the pin holes and small pores, presumably by corrosion products. Even though the χ^2 values (**Table 2**), were high for the early exposure up to 140 min, these EIS data could be used to bring about the evolution of the corrosion of the TiN during the pitting formation and growth.

Before visual observation of the pits based on their brownish colour on the surface (**Figure 10**) (formation of pitting state), the capacitive response of the surface layer (TiO_2) was believed to be degraded by the penetration of the electrolyte through the defects in the coatings, preferentially along the columnar grain boundaries, the pin holes, the large openings or the voids and droplets to the substrate/coating interface (**Figures 3** and **4**). The work of Cai[26] supported this conclusion. Cai[26] studied the effect of a post-deposition treatment of the TiN-coated steel and stainless-steel substrates with polymethyl methacrylate (PMMA) on corrosion in a 3.5 % NaCl solution. They found a significant improvement in the corrosion resistance because of effectively sealing the open voids or pores associated with the coatings. The pits were believed to form at the defect sites (columnar grain boundaries, pin holes, large openings or voids and droplets) by galvanic coupling between the substrate surface and the TiN coating surface. There was a driving force for the galvanic corrosion since the corrosion potential on the substrate surface was more active than the corrosion potential on the TiN surface (**Figure 5**) in agreement with the data reported by Mendibide,[11] who measured a more noble potential of TiN on the glass surface compared to the steel substrate.

The growth or propagation of pits is clearly documented in **Figures 10** and **11** and both were captured by the PR and EIS data (**Figures 5**, **7**, **9** and **15**). At the pit

areas there was no Ti, indicating that the TiN coating during the pitting did not dissolve. The growth stage of the pit involved the growth of the pit area as a result of the detachment, cracking and spallation of the TiN coating due to the dissolution of the substrate at the TiN/substrate interface with time. Even though a number of pits formed on the TiN coated surface, the corrosion resistance after about 24 h was greater than the corrosion resistance of the substrate. This results indicated that the TiN was inherently resistant to corrosion due to the formation of the n-type semiconductor passive film (presumably TiO_2), as identified by the Mott-Shottky analysis (**Figure 12**).

5 CONCLUSIONS

1. The pitting corrosion of the TiN is directly related to the coating defects and the coating structure. The TiN coatings deposited on the substrate consisted of cubic TiN and a passive n-type oxide (presumably TiO_2) film with flat band potentials of –0.83 V vs. SCE, determined by the Mott-Shottky analysis. The coatings defects were columnar grain boundaries extending to the coating/substrate interface, the droplets, the pin holes and the porosities. These defects were preferential sites for the pitting corrosion.

2. PR and EIS measurement captured the formation and growth of the pitting corrosion. The EIS model used supported the degradation of the coating through pitting, in agreement with visual observations. The corrosion resistance (R_p and R_{total}) decreased suddenly during the pitting corrosion. The pitting corrosion was believed to take place at the defect sites by galvanic corrosion, driven by the corrosion potential differences between the TiN surface and the substrate surface.

3. The corrosion resistance of the TiN-coated substrate was greater than the corrosion resistance of the substrate for about 24 h, even though the corrosion resistance of the substrate (R_p and $R_{passive}$) increased logarithmically as the passive layer grew with time, as indicated by the decreasing Y_0. This result indicated that the TiN coating possessed a significant inherent resistance to corrosion.

4. The PR and EIS measurements used together gave similar polarization resistance results, supporting the accuracy of the EIS data and the EC model used for the substrate and the TiN-coated substrate.

6 REFERENCES

[1] B. Warcholinski, A. Gilewicz, Surface Engineering, 27 (**2011**) 7, 491–497, doi:10.1179/026708410X12786785573355

[2] Y. H. Cheng, T. Browne, B. Heckerman, C. Bowman, V. Gorokhovsky, E. I. Meletis, Surface and Coatings Technology, 205 (**2010**) 1, 146–151, doi:10.1016/j.surfcoat.2010.06.023

[3] J. Bujak, J. Walkowicz, J. Kusinski, Surface and Coatings Technology, 180 (**2004**), 150–157, doi:10.1016/j.surfcoat.2003.10.058

[4] A. Horling, L. Hultman, M. Oden, J. Sjolen, L. Karlsson, Surface and Coatings Technology, 191 (**2005**), 384–392, doi:10.1016/j.surfcoat.2004.04.056

[5] C. Ducros, V. Benevent, F. Sanchette, Surface and Coatings Technology, 163-164 (**2003**), 681-688, doi:10.1016/S0257-8972(02)00656-4

[6] C. J. Tavares, L. Rebouta, B. Almeida, J. Bessa e Sousa, Surface and Coatings Technology, 100–101 (**1998**), 65–71, doi:10.1016/S0257-8972(97)00589-6

[7] C. J. Tavares, L. Rebouta, M. Andritschky, S. Ramos, Journal of Materials Processing Technology, 92-93 (**1999**), 177–183, doi:10.1016/S0924-0136(99)00126-0

[8] L. Hultman, J. E. Sundgren, Structure/property relationships for hard coatings, In: R. F. Bunshah (ed.), Handbook of Hard Coatings, William Andrew Publishing, New York 2001, 108–180

[9] H. A. Jehn, Surface and Coatings Technology, 125 (**2000**), 212–217, doi:10.1016/S0257-8972(99)00551-4

[10] M. Fenker, M. Balzer, H. Kappl, Thin Solid Films, 515 (**2006**) 1, 27–32, doi:10.1016/j.tsf.2005.12.020

[11] C. Mendibide, P. Steyer, J. P. Millet, Surface and Coatings Technology, 200 (**2005**), 109–112, doi:10.1016/j.surfcoat.2005.02.060

[12] M. Urgen, A. F. Cakir, Surface and Coatings Technology, 96 (**1997**), 236–244, doi:10.1016/S0257-8972(97)00123-0

[13] M. A. M. Ibrahim, S. F. Korablov, M. Yoshimura, Corrosion Science, 44 (**2002**), 815–828, doi:10.1016/S0010-938X(01)00102-0

[14] W. J. Chou, G. P. Yu, J. H. Huang, Corrosion Science, 43 (**2001**), 2023–2035, doi:10.1016/S0010-938X(01)00010-5

[15] V. K. William Grips, H. C. Barshilia, V. Ezhil Selvi, Kalavati, K. S. Rajam, Thin Solid Films, 514 (**2006**), 204–211, doi:10.1016/j.tsf.2006.03.008

[16] L. Cunha, M. Andritschky, L. Rebouta, R. Silva, Thin Solid Films, 317 (**1998**), 351–355, doi:10.1016/S0040-6090(97)00624-X

[17] I. Kucuk, C. Sarioglu, Mater. Tehnol., 49 (**2015**) 1, 19–26

[18] C. Liu, Q. Bi, A. Leyland, A. Matthews, Corrosion Science, 45 (**2003**), 1243–1256, doi:10.1016/S0010-938X(02)00213-5

[19] C. Liu, Q. Bi, A. Leyland, A. Matthews, Corrosion Science, 45 (**2003**), 1257–1273, doi:10.1016/S0010-938X(02)00214-7

[20] S. Roy Morrison, Electrochemistry at Semiconductor and Oxidized Metal Electrodes, Plenum Press, New York 1980, doi:10.1007/978-1-4613-3144-5

[21] S. Rudenja, C. Leygraf, J. Pan, P. Kulu, E. Talimets, V. Mikli, Surface and Coatings Technology, 114 (**1999**), 129–136, doi:10.1016/S0257-8972(99)00033-X

[22] D. A. Jones, Principles and Prevention of Corrosion, Prentice hall, Inc., 1992

[23] C. H. Hsu, F. Mansfeld, Corrosion, 57 (**2001**) 9, 747–748, doi:10.5006/1.3280607

[24] Y. H. Yoo, D. P. Le, J. G. Kim, S. K. Kim, P. V. Vinh, Thin Solid Films, 516 (**2008**), 3544–3548, doi:10.1016/j.tsf.2007.08.069

[25] C. He, J. Zhang, J. Wang, G. Ma, D. Zhao, Q. Cai, Applied Surface Science, 276 (**2013**), 667–671, doi:10.1016/j.apsusc.2013.03.151

[26] F. Cai, Q. Yang, X. Huang, L. R. Zhao, Corrosion Engineering, Science and Technology, 46 (**2011**) 4, 368–374, doi:10.1179/147842209X12489567719626